Molecular Physics

Publication details, including instructions for authors and subscription information:
http://www.tandfonline.com/loi/tmph20

Anomalous melting and solid polymorphism of a modified inverse-power potential

Gianpietro Malescio [a] , Santi Prestipino [a] & Franz Saija [b]

[a] Università degli Studi di Messina, Dipartimento di Fisica, Viale F. Stagno d'Alcontres 31, 98166 Messina, Italy

[b] CNR-IPCF, Viale F. Stagno d'Alcontres 37, 98158 Messina, Italy

PLEASE SCROLL DOWN FOR ARTICLE

INVITED ARTICLE

Anomalous melting and solid polymorphism of a modified inverse-power potential

Gianpietro Malescio[a*], Santi Prestipino[a] and Franz Saija[b]

[a]Università degli Studi di Messina, Dipartimento di Fisica, Viale F. Stagno d'Alcontres 31, 98166 Messina, Italy; [b]CNR-IPCF, Viale F. Stagno d'Alcontres 37, 98158 Messina, Italy

We numerically investigate a system of particles interacting through a repulsive pair potential of inverse-power form, modified in such a way that the strength of the repulsion is softened in a range of distances. The solid phases of the system for various levels of softness are identified by computing the zero-temperature phase diagram; then, for each solid phase, the melting line is determined by Monte Carlo simulation. Upon increasing the softness of the potential core, a region appears where melting occurs upon compression at constant temperature ('anomalous' melting) and a number of low-coordinated crystals become stable at moderate pressures. Next, the structural properties of the system for varying core softness are surveyed in the hypernetted-chain approximation, whose accuracy has been positively tested against numerical simulation. For sufficiently high degrees of softness, the radial distribution function shows the typical interplay between two distinct length-scales. In a narrow range of moderate softness, reentrant melting occurs instead with just one length-scale, which shows that the existence of two well-definite length-scales is not the only mechanism for anomalous melting.

Keywords: anomalous melting; solid polymorphism; hypernetted-chain approximation

1. Introduction

The generic features of interatomic interactions are a harsh repulsion at short range, caused by the overlap of the outer electronic shells, and a mild attraction at large interparticle separation arising from multipolar dispersion forces, whose leading term (the dipole–dipole interaction) decays as an inverse power of the distance with exponent $n = 6$ [1]. Mainly for reasons of mathematical convenience also the short-range repulsion is often represented through an inverse-power law with an exponent $n = 12$. A popular interaction model which incorporates the two behaviours is the Lennard-Jones (LJ) potential [2], which provides a remarkably adequate description of the interparticle interaction in rare gases. The LJ potential yields a phase diagram that reproduces the behaviour of typical monatomic substances, with a vapour–liquid critical point, a vapour–liquid–solid triple point, and a melting line with positive dT/dP slope [3].

Radially symmetric interactions, however, do not always give rise to simple phase behaviour like in the LJ case. In the last decade or so, intense investigation has shown that unusual behaviours may arise in systems of spherical particles where the diverging repulsive core is 'softened' through the addition of a finite repulsion at intermediate distances, so as to generate two distinct length-scales: a 'hard' radius, related to the inner core, and a 'soft' radius, associated with the more penetrable component of the repulsion [4–26]. Due to this feature, these so-called core-softened (CS) fluids are characterized by two competing, expanded and compact, local particle arrangements. This property, though arising from simple isotropic interactions, mimics the behaviour of the more complex network-forming fluids (such as, *e.g.*, water) where the loose and compact local structures arise from the continuous formation and disruption of the dynamic network generated by directional bonds [27]. Similarly to network-forming fluids, CS systems may show anomalous (reentrant) melting, *i.e.*, melting upon compression at constant temperature, which implies a negative dT/dP slope of the melting line, polymorphism in the liquid and solid phases, as well as a number of anomalous behaviours in the fluid, like a density anomaly (a decrease in the number density upon isobaric cooling), a diffusion anomaly (an increase of diffusivity upon isothermal compression), and a structural anomaly (a decrease of structural order, as measured, *e.g.*, by the pair entropy, for increasing pressure at fixed temperature). Recently, it has been shown that a very weak softening of the repulsive interparticle interaction, though unable to yield two distinct length-scales, can nevertheless give rise to anomalous behaviours [28]. This evidence

---

challenges the idea that the existence of two length-scales is essential for the occurrence of anomalous behaviours and suggests that the class of isotropic interactions that may generate such behaviours is wider than commonly assumed.

In this paper, we investigate the effects of gradually softening an inverse-power repulsive interaction. By making use of numerical simulation and of the hypernetted-chain integral equation, we study how the behaviour of the system varies as the repulsion softening becomes more and more strong. This makes it possible to follow the onset of water-like anomalies until their full development and, in particular, it enables us to see the crossover from the one-scale behaviour typical of standard LJ-like fluids to the two-scale behaviour characterizing the CS systems.

2. Model

Since we plan to focus on anomalous melting and solid polymorphism as the main features of anomalous phase behaviour [29], our analysis will be limited to systems with purely repulsive interactions. We consider a family of modified inverse-power (MIP) potentials where the exponent n depends on the interparticle distance r in such a way as to make the repulsion milder in a range of distances:

$$u_{MIP}(r) = \epsilon(\sigma/r)^{n(r)}, \qquad (1)$$

where ϵ and σ are energy and length units and

$$n(r) = n_0\{1 - a\exp[-b(1 - r/\sigma)^2]\}. \qquad (2)$$

Here, a is a number between 0 and 1, and b is positive. The parameter a controls the repulsion softening: the greater the value of a, the more substantial the softening effect is, *i.e.*, the higher the local reduction of $n(r)$. The exponent $n(r)$ attains its minimum $n_{min} = n_0(1 - a)$ at $r = \sigma$. The parameter b governs the width of the interval where $n(r)$ is significantly smaller than n_0: the larger b is, the smaller this interval is. In the following, we choose $n_0 = 12$ and $b = 5$. For $a = 0$ the potential in Equation (1) has a purely inverse-power form, *i.e.*, $u(r) = \epsilon(\sigma/r)^{n_0}$ and there is only one solid phase with FCC symmetry. As a increases, $u_{MIP}(r)$ becomes less and less steep in a range of distances centred around $r = \sigma$ until, for $a = 1$, $u_{MIP}(r)$ shows an inflection point with zero slope in $r = \sigma$ (see Figure 1). As a approaches 1, $u_{MIP}(r)$ develops a downward concavity in a range of r, a feature that is typical of CS potentials.

In the region where a repulsive potential $u(r)$ shows a downward or zero concavity, the strength of the two-body force $f(r) = -u'(r)$ decreases or at most remains
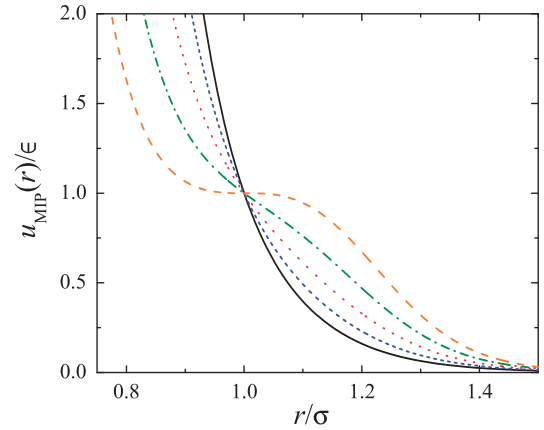

Figure 1. The potential $u_{MIP}(r)$ for several values of a: $a = 0.2$ (black solid line), 0.4 (blue dashed line), 0.6 (red dotted line), 0.8 (green dashed-dotted line), and 1 (orange long-dashed line).

constant as the two particles approach each other. Assuming that $u(r)$ is diverging at small distances, it is possible to identify two different regions where the force increases as r gets smaller. Thus, two distinct repulsive length-scales emerge: a smaller hard-core radius, which is dominant at high pressures, and a larger soft-core radius, which is effective at low pressure. In the range of pressures where the two length-scales compete with each other, the system behaves as a 'two-state' fluid. In mathematical terms core softening was expressed by Debenedetti *et al.* [30] through the condition $\Delta[rf(r)] < 0$ for $\Delta r < 0$ in some interval $r_1 < r < r_2$, with $u''(r) > 0$ for $r < r_1$ and $r > r_2$. This implies that, in the interval between r_1 and r_2, the product $rf(r)$ (rather than just $f(r)$) gets smaller with decreasing interparticle separation. This requirement is less restrictive than the condition $u''(r) \leq 0$ and can be met also by a strictly convex potential, provided that in a range of distances the force increases more slowly than in the adjacent regions [23]. The MIP potential shows a downward concavity for $a \geq 0.72$ while the Debenedetti condition is satisfied for $a \geq 0.68$. Recently, a criterion stating a necessary condition for the occurrence of reentrant melting has been presented [31]. According to this criterion, anomalous melting is possible for the MIP potential when $a \geq 0.47$.

3. Method

To estimate the melting line, we performed Monte Carlo (MC) simulations in the isothermal-isobaric NPT ensemble, *i.e.*, at constant temperature T, pressure P, and number N of particles, using the standard

Metropolis algorithm with periodic boundary conditions. The simulations were carried out for a number of particles ranging from $N = 686$ for a body-centred cubic (BCC) crystal to $N = 864$ for a face-centred cubic (FCC) crystal (we checked that finite-size effects are negligible). At a given pressure, we typically generate a sequence of simulation runs starting at low temperature from a perfect crystal. This series of runs is continued until a sudden density/energy change is observed. Since the density of a solid ordinarily varies very little with increasing temperature along an isobar, a sudden density change indicates a mechanical instability of the solid in favour of the fluid, and thus marks approximately the location of melting, as is also confirmed by the concurrent rounding off of the peaks of the radial distribution function (RDF). In fact, by this so-called 'heat-until-it-melts' (HUIM) method one just determines the upper stability threshold of the solid when heated isobarically. The reliability of the HUIM approach as a means to locate the coexistence of fluid and solid has been recently tested against 'exact' free-energy calculations for a couple of softened-core fluids and found to be good (see Ref. [21,23,28] for details). In any event, our use of the HUIM method is especially directed to obtain the topology of the melting line and to locate the threshold in a between the regimes of standard and anomalous melting. In this respect, the HUIM method represents a satisfactory approach.

In order to study how the structural properties of the MIP fluid change as the interaction is gradually softened, it is convenient to have a fast method to calculate the RDF. Such a method may be provided by integral-equation theories. In particular, we consider the hypernetted-chain (HNC) approximation, consisting of solving the Ornstein–Zernike relation by using the HNC closure [1]:

$$g(r) = \exp[-\beta u(r) + h(r) - c(r)], \qquad (3)$$

where $g(r)$ is the RDF, $h(r) = g(r) - 1$, $c(r)$ is the direct correlation function, and $\beta = 1/(k_B T)$. We will show in the following that the HNC theory is surprisingly good for the MIP fluid.

A distinctive feature of systems with softened interparticle repulsion is a rich solid polymorphism, *i.e.*, the existence of many different stable crystal phases at low temperature. In systems with unbounded interparticle repulsion, this multiplicity of phases occurs because of the frustration of highly-coordinated packings at intermediate pressures, which opens the way to observing 'unusual' particle arrangements of moderately high density and low coordination number. Eventually, upon further compression, the harsh inner core of the potential comes into play and the FCC order takes over. When investigating the melting behaviour, solid polymorphism represents a complication since the number of crystals that are potentially relevant for the system at hand is enormous. A common simplification consists in restricting the calculation of the chemical potential to just those phases that are found stable or nearly stable at zero temperature, where obtaining the chemical potential as a function of pressure is a rather straightforward task. Hence, we performed an analysis of the zero-temperature phase diagram of the system as a function of the softness parameter by examining a large number of crystal structures. The outcome of this calculation is used as a guide for computing, through the HUIM method, the melting temperature of the system as a function of the pressure P.

4. Results

At $T = 0$ and fixed pressure, a crystal phase is thermodynamically stable if its enthalpy is smaller than that of any other phase. However, the problem of minimizing the enthalpy among all crystals is a formidable task, since the number of possible structures is virtually infinite. Hence, we restrict the search for stable structures to a limited – albeit large – number of candidates, including, aside from Bravais crystals, also a number of Bravais lattices with a basis (non-Bravais crystals). Enthalpy minimization is achieved by adjusting the crystal density and, for some of the analysed crystal lattices, also a structure parameter.

In Table 1, the zero-temperature phases of the MIP fluid are reported for a number of a values. Overall, we see that the softer the potential, the richer the solid polymorphism. Upon increasing a up to 0.8, a non-Bravais crystal (β-Sn, with fourfold coordination) becomes eventually stabilized at moderate pressures. In fact, the preference for low-coordinated crystals at intermediate pressures seems to be a general feature among CS potentials, while the close-packed FCC structure is stable only for the low and the very high pressures [32]. Obviously, we cannot exclude the existence of other phases that are more stable than those found in our calculation; yet, the conclusion that the coordination number shows a dip for intermediate pressures remains valid even if some of the phases that we call stable are actually metastable (note that the high-coordinated crystals are all among the reviewed phases). In Figure 2, the chemical potential of the relevant phases for $a = 0.8$ is plotted as a function of the pressure P, assuming the FCC solid as reference. We see that, in its own range of stability, the β-Sn solid

Table 1. MIP potential, zero-temperature phase diagram up to $P = 20\,\epsilon\sigma^{-3}$ for a number of a values. For each phase (column 2), we report the pressure interval of stability (column 1, units of $\epsilon\,\sigma^{-3}$), the corresponding density interval (column 3, units of σ^{-3}), and the values of the structure parameter (if any is present; column 4). The scrutinized lattices were the following: FCC, BCC, HCP, SC, diam, BC8, cI16-Li, β-Sn, SH, ST, BCT, graphite (see Ref. [32] for the notation employed).

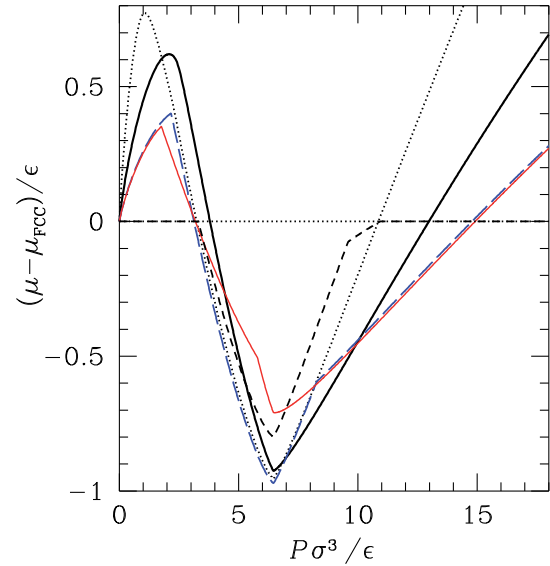|			
$a = 0.5$			
0–2.91	FCC	0–0.729	–
2.92–11.91	BCC	0.739–1.210	–
11.92–20	FCC	1.229–1.464	–
$a = 0.55$			
0–2.83	FCC	0–0.705	–
2.84–11.14	BCC	0.717–1.200	–
11.15–11.72	BCT	1.204–1.233	0.92–0.87
11.73–20	FCC	1.254–1.510	–
$a = 0.6$			
0–2.85	FCC	0–0.688	–
2.86–6.32	BCC	0.701–0.948	–
6.33–7.88	BCT	0.958–1.040	1.95–1.93
7.89–13.00	SH	1.096–1.287	0.94–0.97
13.01–20	FCC	1.352–1.563	–
$a = 0.8$			
0–3.12	FCC	0–0.631	–
3.13–6.98	β-Sn	0.850–1.019	0.77–0.80
6.99–9.89	SC	1.118–1.218	–
9.90–14.91	SH	1.315–1.454	1.06–1.05
14.92–20	FCC	1.674–1.801	–

Figure 2. MIP potential for $a = 0.8$: zero-temperature chemical potential μ, plotted as a function of the pressure P, for a number of crystal structures (the FCC lattice was taken as reference; both μ and P are in reduced units; the chemical potentials of structures that are never stable are not shown, except for the BC8 and BCT phases). Besides FCC, the stable phases are β-Sn (long dashed blue line), SC (thick solid black line), and SH (thin solid red line). The BC8 and BCT chemical potentials are plotted as black dotted and dashed lines, respectively; between $P = 3$ and $P = 6$, they are only slightly larger than the chemical potential of β-Sn. Between $P \approx 2$ and $P \approx 8$, the BC8 phase is nearly degenerate with β-Sn. Similarly, between $P \approx 8$ and $P = 20$, the SC and β-Sn phases have approximately the same chemical potentials.

is almost degenerate with a BC8 phase, signalling that the latter phase may become stable at $T > 0$ just for entropic reasons. In a similar way, the β-Sn crystal is nearly as stable as the simple cubic (SC) crystal at still higher pressures, leaving the possibility of a phase transition from SC to β-Sn at some non-zero temperature. On account of this, we included also the BC8 crystal in the list of phases to be analysed later, for $a = 0.8$, by the HUIM method.

Computer-simulation results show (see Figure 3) that, as a increases, the melting line gradually turns from a monotonically increasing behaviour ($a = 0.5$) to a non-monotonic one where a local maximum is followed by a region of reentrant melting ($a = 0.6$). Correspondingly, the phase portrait becomes rich, with solid phases other than FCC and BCC. For a considerably softened repulsion ($a = 0.8$), the melting line has a complex shape with multiple maxima and reentrant regions while the system displays water-like anomalies in the fluid phase [31]. For this a value, the stable phases for $T > 0$ are, besides a low-pressure FCC crystal, also a non-Bravais crystal (β-Sn) followed, at higher pressures, by a simple-cubic solid. We checked that, between $P = 3$ and $P = 7$, the BC8 and

body-centred tetragonal (BCT) solids would melt at a temperature lower than the melting temperature for β-Sn, which is consistent with their status of metastable phases.

For two selected values of a (i.e., $a = 0.6$ and $a = 0.8$), we calculated the RDF along the $T = 0.2\,\epsilon/k_B$ path and compared the results with those got from the HNC approximation. As shown in Figures 4 and 5 the HNC approximation is reasonably accurate. The main discrepancies are observed for intermediate pressures, where the height of the RDF peak corresponding to the soft radius is slightly underestimated, while the height of the peak relative to the hard radius is slightly overestimated at low pressures. However, all differences turn out to be smaller than 10%. Aside from these minor deviations, the HNC theory is nonetheless able to reproduce accurately the qualitative changes occurring in the local structure of the system when varying the level of repulsion softening. Moreover, in spite of the thermodynamic inconsistency of the HNC theory, the pressure computed using the virial route is quite close to the simulation value (see Table 2).
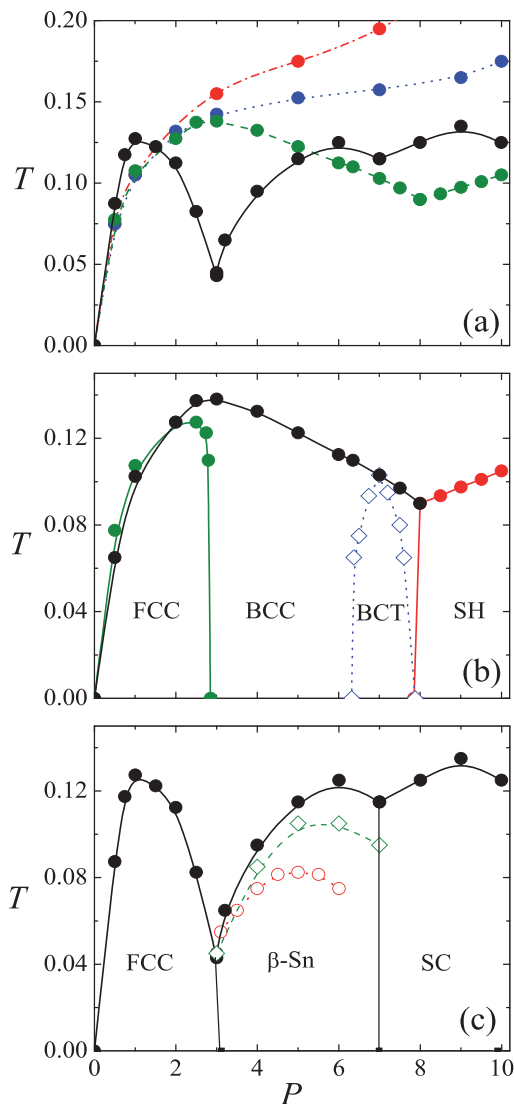
Figure 3. Phase diagram of the MIP potential. (a) HUIM melting line for a number of a values: $a = 0.5$ (red dash dotted line), 0.55 (blue dotted line), 0.6 (green dashed line), and 0.8 (black solid line). The error bars are of the same size as the dots. (b) $a = 0.6$, HUIM loci for selected solid phases. The BCT phase (blue line) is stable at $T = 0$ but, upon heating, it melts at a temperature lower than the BCC one (black line). This suggests the existence of a BCT-BCC transition before melting. (c) Phase diagram for $a = 0.8$. The red and green curves are the HUIM melting lines for the BCT and BC8 solids, respectively. These solids are metastable at $T = 0$; accordingly, their melting temperature turns out to be lower than that of the β-Sn solid.

Given the accuracy of the HNC approximation in the present case, we used this theory to obtain an overall picture of the softening-induced structural modifications in the MIP fluid (see Figure 6). For $a = 0.6$ (Figure 6a) the pressure behaviour of the RDF is intermediate between that typical of CS fluids and the one characteristic of standard inverse-power

repulsive interactions. As P increases at constant temperature, the nearest-neighbour peak of $g(r)$ gradually moves towards small r. Meanwhile its height first grows, due to the increasing proximity with the solid lying at lower temperature, and then goes down in the pressure range where reentrant melting occurs. As P increases further, the peak grows again while its position changes less and less sensibly due to the small-r steep repulsion. This behaviour is consistent with the existence of just one effective length-scale that shrinks with pressure (a feature typical of inverse-power potentials); at the same time, the rise and fall with pressure of the height of the main $g(r)$ peak is reminiscent of the order–disorder interplay related to the occurrence of reentrant melting (a feature characterizing CS fluids).

As a gets larger, the soft length-scale becomes better and better defined. The first peak of $g(r)$ starts bifurcating (Figure 6b and c) until, for $a = 0.8$ (Figure 6d), it splits into two well-distinct peaks corresponding to the hard and the soft radius, respectively. Like for CS interactions, the heights of these peaks change in opposite directions on increasing pressure, the first peak becoming higher and higher while the second peak gradually gets lower. This behaviour signals the coexistence in the system of two populations of particles having distinct effective diameters. As the pressure goes up, the hard-core radius (associated with the first RDF peak) becomes more and more populated at the expense of the soft-core radius (associated with the second peak), whereas the positions of the two peaks, *i.e.*, the two length-scales, remain essentially unaltered.

5. Concluding remarks

In recent years, increasing attention has been paid to soft-matter systems as real examples of anomalous thermodynamic and structural behaviours. Much effort has been devoted to the investigation of simple isotropic model systems which, through the softening of the repulsive component of the particle interaction, are able to display such anomalous behaviours. The study of these systems may help to unveil the statistical mechanisms that are responsible for these anomalies. This research is relevant also for the physics of elemental solids under extreme conditions, where anomalous melting and solid polymorphism are observed as a result of pressure-induced rearrangements in the electronic structure [21].

In this paper we studied the phase behaviour of a family of potentials with tunable core softness, finding elements of complexity that are simply
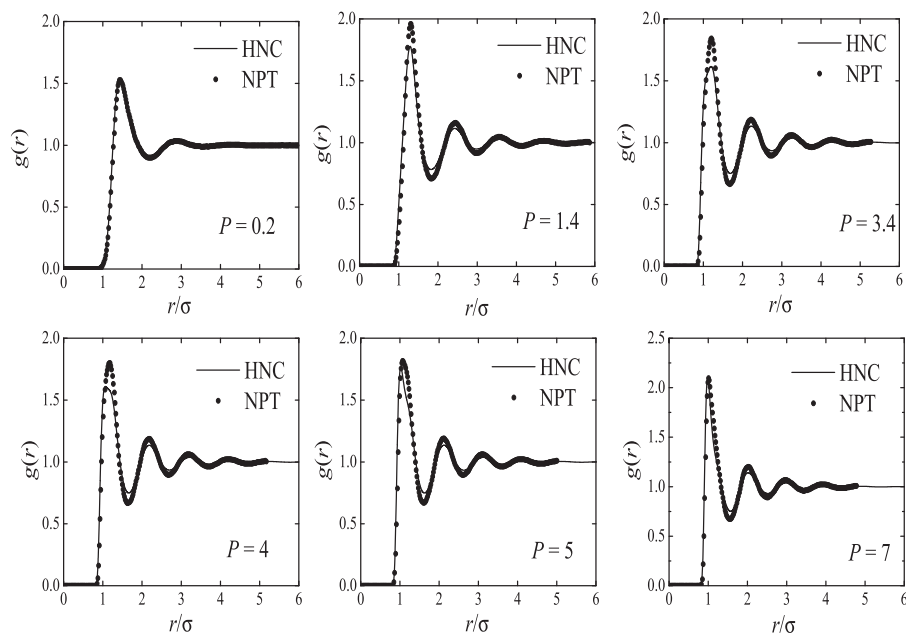
Figure 4. MIP potential, radial distribution function $g(r)$ as computed from the HNC theory (solid lines) and from MC simulation (dots) for $a = 0.6$ and six pressures (the reduced temperature is $T = 0.2$).
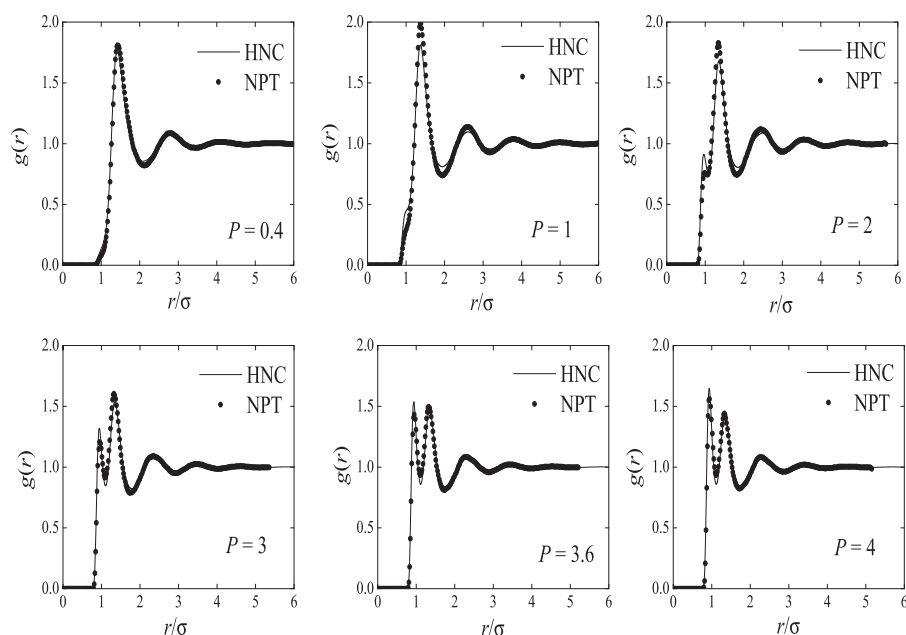

Figure 5. MIP potential, radial distribution function $g(r)$ as computed from the HNC theory (solid lines) and from MC simulation (dots) for $a = 0.8$ and six pressures (the reduced temperature is $T = 0.2$).

unknown to 'normal' systems like the Lennard-Jones and inverse-power fluids. In particular, we found clear evidence that low-coordinated (even non-Bravais) lattices do provide the structure of stable solid phases at intermediate pressures. In the coming years, as the techniques to functionalize the surface of colloidal particles gradually improve, it will become possible to realize soft materials characterized by effective interparticle potentials similar to the one investigated here and thus able to yield a spontaneous assembly of particles into non-Bravais structures.

Table 2. MIP potential, system pressures (in units of $\epsilon\sigma^{-3}$) computed through the HNC equation and MC simulation for various densities, at the reduced temperature $T=0.2$.

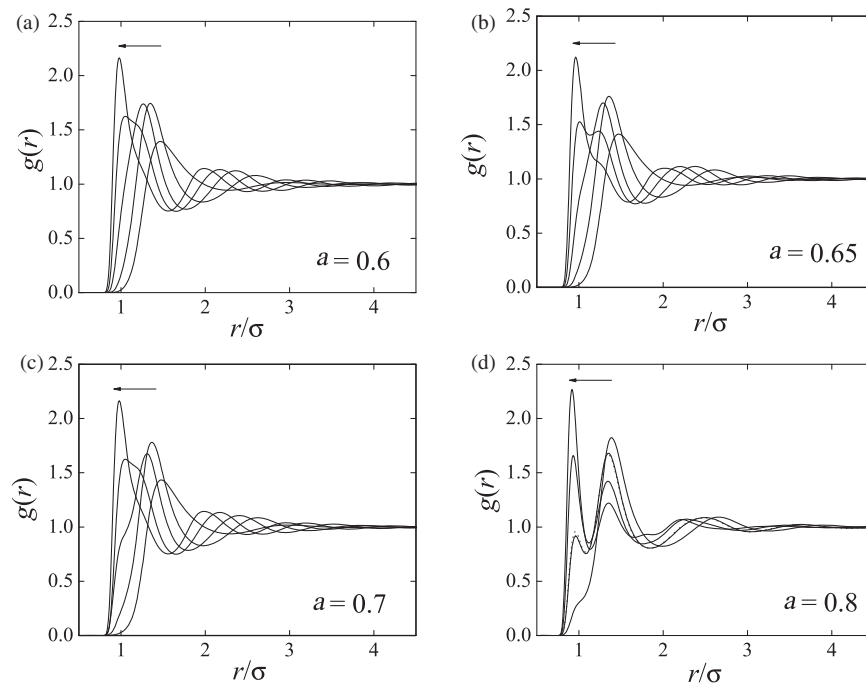|	$a=0.6$			$a=0.8$	
$\rho\sigma^3$	P (HNC)	P (MC)	$\rho\sigma^3$	P (HNC)	P (MC)
0.2601	0.211	0.2	0.3225	0.425	0.4
0.5348	1.454	1.4	0.4480	1.013	1.0
0.7366	3.452	3.4	0.5871	1.969	2.0
0.7834	4.058	4.0	0.7013	2.978	3.0
0.8539	5.082	5.0	0.7617	3.595	3.6
0.9740	7.151	7.0	0.7991	4.006	4.0

Figure 6. MIP potential, radial distribution function $g(r)$ for $T=2$ in the HNC approximation. Various a values are considered ($a = 0.6, 0.65, 0.7, 0.8$). The arrows mark the direction of pressure increase. For each a, $g(r)$ refers to $\rho = 0.2, 0.4, 0.6, 0.8$, and 1 (in units of σ^{-3}), the respective pressures being reported in Table 3.

Table 3. MIP potential, system pressures (in units of $\epsilon\sigma^{-3}$) computed through the HNC equation as a function of the density for various a values (the reduced temperature is $T=0.2$).

$\rho\sigma^3$	$a=0.6$	$a=0.65$	$a=0.7$	$a=0.8$
0.2	0.117	0.120	0.123	0.130
0.3	0.301	0.312	0.324	0.351
0.4	0.648	0.675	0.702	0.754
0.5	1.206	1.246	1.282	1.335
0.6	1.993	2.029	2.056	2.073
0.7	3.016	3.025	3.020	2.966
0.8	4.287	4.242	4.180	4.017
0.9	5.825	5.694	5.549	5.234
1.0	7.658	7.403	7.144	6.628

Another significant point of our investigation concerns the analysis of the changes in the local structure of the system as the repulsion is gradually softened, going from the inverse-power form to that typical of CS potentials. For weak repulsion softening, a reentrant-fluid region appears in the melting line while the radial distribution function $g(r)$ still exhibits a single pressure-modulated length-scale. Only when the level of softening becomes significant, does $g(r)$ acquire the two-scale aspect typical of CS systems. This outcome confirms that the 'two-scale' mechanism is not strictly necessary for explaining the occurrence of anomalous behaviours in systems with isotropic interactions [28].

2844 *G. Malescio* et al.

References

[1] J.P. Hansen and I.R. McDonald, *Theory of Simple Liquids* (Academic Press, London, 1976).

[2] J.E. Lennard-Jones, Proc. Camb. Phil. Soc. **27**, 469 (1931).

[3] D.A. Young, *Phase Diagrams of the Elements* (University of California, Berkeley, 1991).

[4] P.C. Hemmer and G. Stell, Phys. Rev. Lett. **24**, 1284 (1970).

[5] M.R. Sadr-Lahijany, A. Scala, S.V. Buldyrev and H.E. Stanley, Phys. Rev. Lett. **81** (1998).

[6] E.A. Jagla, Phys. Rev. E **58**, 1478 (1998).

[7] M. Watzlawek, C.N. Likos and H. Löwen, Phys. Rev. Lett. **82**, 5289 (1999).

[8] G. Franzese, G. Malescio, A. Skibinsky, S.V. Buldyrev and H.E. Stanley, Nature **409**, 692 (2001).

[9] G. Franzese, G. Malescio, A. Skibinsky, S.V. Buldyrev and H.E. Stanley, Phys. Rev. E **66**, 051206 (2002).

[10] G. Malescio, G. Franzese, G. Pellicane, A. Skibinsky, S.V. Buldyrev and H.E. Stanley, J. Phys.: Condens. Matter **14**, 2193 (2002).

[11] G. Malescio and G. Pellicane, Nature Mat. **2**, 97 (2003).

[12] A. Skibinsky, S.V. Buldyrev, G. Franzese, G. Malescio and H.E. Stanley, Phys. Rev. E **69**, 061206 (2004).

[13] G. Malescio and G. Pellicane, Phys. Rev. E **70**, 021202 (2004).

[14] G. Malescio, G. Franzese, A. Skibinsky, S.V. Buldyrev and H.E. Stanley, Phys. Rev. E **71**, 061504 (2005).

[15] Z. Yan, S.V. Buldyrev, N. Giovambattista and H.E. Stanley, Phys. Rev. Lett. **95**, 130604 (2005).

[16] H.M. Gibson and N.B. Wilding, Phys. Rev. E **73**, 061507 (2006).

[17] G. Malescio, J. Phys.: Condensed Matter **19**, 073101 (2007).

[18] Y.D. Fomin, N.V. Gribova, V.N. Ryzhov, S.M. Stishov and D. Frenkel, J. Chem. Phys. **129**, 064512 (2008).

[19] Y.D. Fomin, E.N. Tsiok and V.N. Ryzhov, J. Chem. Phys. **134**, 044523 (2011).

[20] G.J. Pauschenwein and G. Kahl, Soft Matter **4**, 1396 (2008).

[21] G. Malescio, F. Saija and S. Prestipino, J. Chem. Phys. **129**, 241101 (2008).

[22] A.B. de Oliveira, P.A. Netz and M. Barbosa, Europhys. Lett. **85**, 36001 (2009).

[23] F. Saija, S. Prestipino and G. Malescio, Phys. Rev. E **80**, 031502 (2009).

[24] P. Vilaseca and G. Franzese, J. Chem. Phys. **133**, 084507 (2010).

[25] E. Lascaris, G. Malescio, S.V. Buldyrev and H.E. Stanley, Phys. Rev. E **81**, 031201 (2010).

[26] O. Mishima and H.E. Stanley, Nature **396**, 329 (1998).

[27] P.G. Debenedetti, *Metastable Liquids* (Princeton University Press, Princeton, 1996).

[28] S. Prestipino, F. Saija and G. Malescio, J. Chem. Phys. **133**, 144504 (2010).

[29] P.F. McMillan, J. Mater. Chem. **14**, 1506 (2004).

[30] P.G. Debenedetti, V.S. Raghavan and S.S. Borick, J. Phys. Chem. **95**, 4540 (1991).

[31] G. Malescio and F. Saija, J. Phys. Chem. B (2011) accepted.

[32] S. Prestipino, F. Saija and G. Malescio, Soft Matter **5**, 2795 (2009).